



Technische Universität München  
Department of Electrical Engineering and Information Technology  
Bio-Inspired Information Processing

Bachelor's Thesis

# Investigation of Cortical Responses to Modulated Noise Stimuli Using fNIRS

Pei-Yi Lin

*Date of Submission:*  
September 10, 2022

*Supervisors:*  
Prof. Dr.-Ing. Werner Hemmert  
Dr. Ali Saeedi  
M.Sc. Carmen Marie Castañeda González



## **Abstract**

Write your abstract here or use \input{} command.



# Acknowledgments

Thanks people!



# Contents

<b>1</b>	<b>Introduction</b>	<b>1</b>
1.1	Motivation . . . . .	1
1.2	Technical Background . . . . .	2
1.3	Related Work . . . . .	3
<b>2</b>	<b>Methods</b>	<b>4</b>
2.1	Study Participants . . . . .	4
2.2	Probe Design . . . . .	4
2.3	Acoustic Stimulation during fNIRS Experiment . . . . .	7
2.4	fNIRS Setup . . . . .	8
2.5	Data preprocesing . . . . .	9
<b>3</b>	<b>Results</b>	<b>13</b>
3.1	Waveform Morphology . . . . .	13
3.1.1	Oxygenated Hemoglobin, HbO . . . . .	14
3.1.2	Deoxygenated Hemoglobin, HbR . . . . .	17
3.2	Region of Interest . . . . .	19
3.3	Poor Measurements . . . . .	22
<b>4</b>	<b>Discussion</b>	<b>23</b>
4.1	Participant 3 . . . . .	23
4.2	Participant 5 . . . . .	23
4.3	Participant 6 . . . . .	23
4.4	Participant 7 . . . . .	24
4.5	Participant 8 . . . . .	24
4.6	Regional Analysis . . . . .	24
<b>5</b>	<b>Conclusion and Future Prospectives</b>	<b>25</b>
<b>List of Figures</b>		<b>28</b>
<b>List of Tables</b>		<b>29</b>

*Contents*

**References**

**31**

# Chapter 1

## Introduction

### 1.1 Motivation

This research is aimed for better understanding of the brain activities when the subjects are exposed to different audio stimuli with the help of fNIRS measurement.

In the field of neuro-imaging, although fMRI is widely used and provides excellent (spatial) resolution, it still has many limitations, especially when it comes to hearing research. First of all, MRI rooms are noisy, which makes it difficult to control the audio stimulation desired due to inevitable environmental noises. In addition, fMRI scans are done in a magnetic field. It has not yet been proved that pregnant women and infants can be safely exposed to an external magnetic field in the MRI room. For people with hearing disabilities, more specifically cochlear implant patients, going into a MRI room would not be ideal, either. Although there are already cochlear implants that can be worn to a magnetic field, it is still generally not suggested to wear a piece of metal in a MRI room.

fNIRS, short for functional near-infrared spectroscopy. With fNIRS, we can measure brain activity by using near-infrared light to estimate cortical hemodynamic activity which occur in response to neural activity. It is non-invasive and risk-free. The fNIRS device is portable and works silently. With the cap secured on the head, it is also more resilient to motion artifacts. All these makes it ideal for hearing researches. However, it is not yet commonly used in clinical diagnostics due to the lack of understanding of the expected brain activities measured with fNIRS. Therefore, in this research, we'd like to perform some fNIRS measurement and analyse the fNIRS data under different experiment conditions.

If fNIRS can provide more meaningful data and be more commonly used

## *Introduction*

in early clinical diagnosis, we may find hearing abnormality of patients earlier. This is especially important for infants or children. As language development happens in the early stages of one's life, the sooner we find the hearing abnormality and fix it, the better. After a child turns 8, it is practically not possible for him to understand human speech even with perfect hearing. I personally find hearing research a meaningful topic. For one, speech is the primary and direct way of human communication. We express ourselves and perceive other people's opinion via speech. For the other, music has always been an important part of my life for me personally. Without the ability to hear and listen, neither speech nor music will be possible to be perceived. Therefore, I want to help other people with hearing disabilities get better diagnosis and treatment. fNIRS is of great potential to help solve the issue.

## **1.2 Technical Background**

Hemoglobin, the protein from inside red blood cells, transports oxygen molecules throughout the body. Higher hemoglobin levels and red blood cell transfusion are associated with higher cerebral oxygen delivery. Different concentration levels of hemoglobin results in a spectral change. The biological tissue has a relatively good transparency for light in the near-infrared region (700-1300nm) [Jöbsis, 1977]. Therefore, it's possible to transmit sufficient photons *in situ* monitoring.

The technique of NIRS relies on the Beer-Lambert law, which is given by:

$$OD_\lambda = \log\left(\frac{I_0}{I}\right) = \epsilon_\lambda \cdot c \cdot L$$

$OD_\lambda$ : a dimensionless factor known as the optical density of the medium.

$I_0$  : the incident radiation.

$I$ : the transmitted radiation.

$\epsilon_\lambda$ : the molar absorptivity ( $mM^{-1} \cdot cm^{-1}$ ) of the chromophore.

$c$ : the concentration ( $mM$ ) of the chromophore.

$L$ : length of light path.

The Beer-Lambert law was intended for use in a clear, non-scattering medium. When the law is applied to a scattering medium, e.g. brain tissue, a correction factor should be applied. The factor, called "differential path-length factor (DPF)" accounts for the increase in optical path length due to scattering in the tissue. The modified Beer-Lambert law is given by:

$$OD_\lambda = \epsilon_\lambda \cdot c \cdot L \cdot B + OD_{R,L}$$

### 1.3 Related Work

where  $OD_{R,L}$  represents the oxygen-independent light absorption due to scattering in the tissue, and  $(L \cdot B)$  is the true mean pathlength traveled by the detected photons. In our case, i.e. CW-NIRS, this mean pathlength is not known. In a highly scattering medium, the pathlength of trajectories is longer than the source-detector separation. Nevertheless, one may still estimate the pathlength within the whole sampling region by multiplying the source-detector distance with a DPF. Assuming  $OD_{R,L}$  is constant during a measurement, we may rewrite the previous equation in terms of changes in optical density and changes in concentration as follows:

$$\Delta c = \frac{\Delta OD_\lambda}{\epsilon_\lambda \cdot L \cdot B}$$

The validity of the above equation depends on how much B varies. [Delpy et al., 1988] investigated this question and gave a relation between the DPF and the head diameter. Nonetheless, newer research also provides different ways to estimate the DPF. In the scope of this project, the DPF was calculated from a function of wavelengths and age of the participant [Duncan et al., 1996].

## 1.3 Related Work

Delpy: MBLL

A. Duncan: DPF

Weder et al.: main paper

Wavelet for MA: <https://iopscience.iop.org/article/10.1088/0967-3334/33/2/259/pdf>

Sato: extracebrellel components remove

This project is based on the previous study [Weder et al., 2018]. The authors measured their human subjects with fNIRS when the subjects were given different sound stimuli with different sound pressure levels. In their research, the results showed that fNIRS responses originating from auditory processing areas are highly dependent on sound intensity level. More specifically, higher stimulation levels led to higher concentration changes. Caudal and rostral channels showed different waveform morphologies, reflecting specific cortical signal processing of the stimulus.

# Chapter 2

## Methods

### 2.1 Study Participants

We measured 8 normal hearing people. Participant 8 was given silent stimuli as a comparison. The detailed information about the subjects are listed in the table.

Participant	Gender	Handedness	Race	Hair color	Age
1 chang	F	right-handed	east asian	dark	22 yr
2 gleb	M	right-handed	caucasian	blond	18
3 jonas	M	left-handed	caucasian	brunet	21
4 lin	F	right-handed	east asian	dark	21
5 lukas	M	right-handed	caucasian	blond	26
6 shelia	F	right-handed	southeast asian	dark	22
7 liao.	M	left-handed	east asian	dark	23
8 luca	M	right-handed	caucasian	blond	22

Table 2.1: Study Participants.

### 2.2 Probe Design

The probes were first designed in AtlasViewer [pic] [Aasted et al., 2015] and the SD GUI interface. I tried to replicate the probe design as close as possible to the research from Weder et al. However, several modifications need to be made due to device limitations.

First of all, the paper only provided a rough 2D-sketch of their probe design. [see pic] The channels were not described in detail. Though there are

## 2.2 Probe Design

different ways to define the channels, we believe it shouldn't matter as long as the mid-points of the channel correspond to that of the previous research.

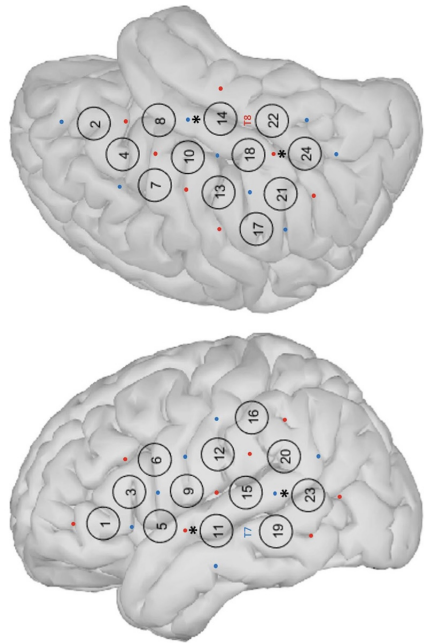


Figure 2.1: Probe design from Weder et al.

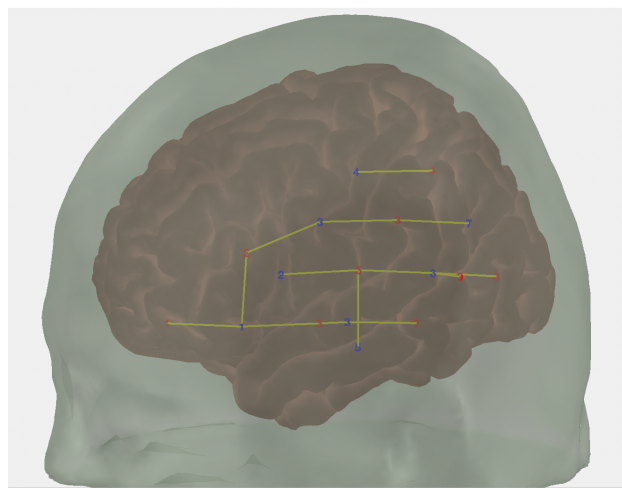


Figure 2.2: Probe design in this research. Shown in AtlasViewer. The red numbers represent the light sources and the blue numbers represent the detector. Channels are shown in yellow lines.

## Methods

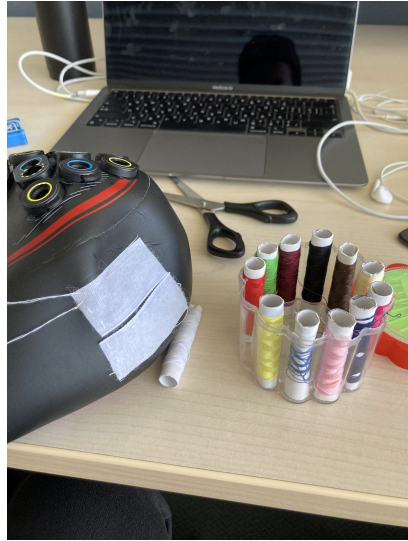


Figure 2.4: Manufacturing process of the cap



Figure 2.5: Finished cap on dummy

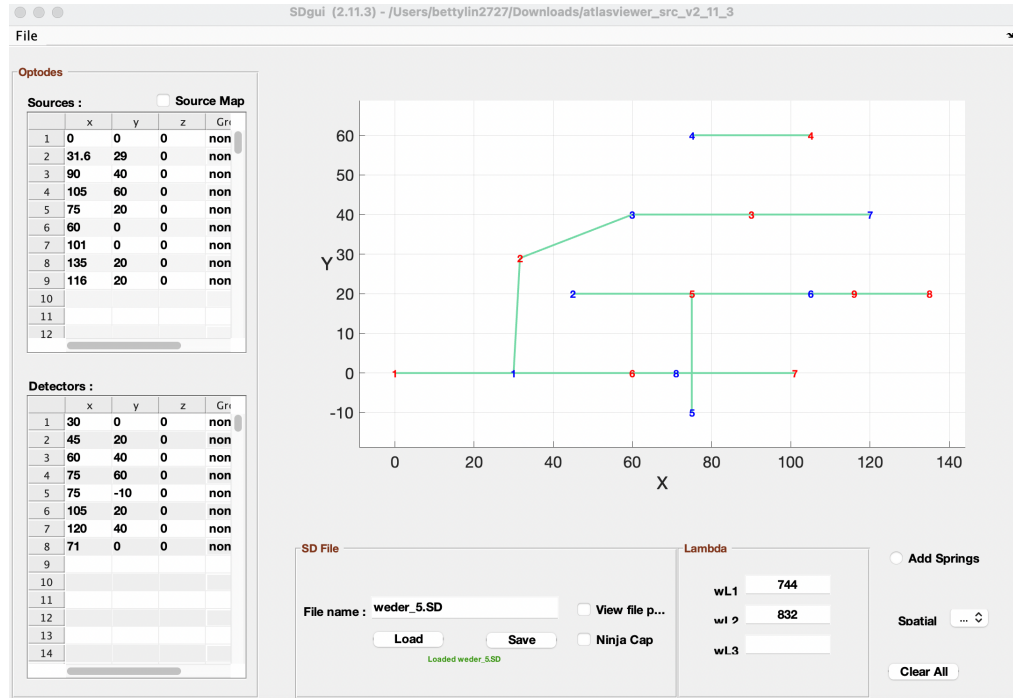


Figure 2.3: SDgui interface and optode coordinates.

Due to device limitations, we only measured one side of the brain. According to previous research [Frost et al., 1999], language processing has

### *2.3 Acoustic Stimulation during fNIRS Experiment*

been predominantly associated to cortical activity in the left hemisphere. As a result, we've decided to focus on the left hemisphere.

The fNIRS device we use also has limited number of sources and detectors. If we'd like to keep the original design, we'd need 9 sources and 9 detectors. However, the device we are using has only 10 sources and 8 detectors. Hence, we shifted one channel around T7 a little bit to the left, so that one less detector is needed. At the end, there were 12 long channels and 2 short channels in our setup.

For the software usage, an .xml file is required. In the .xml file, the sources, detectors, and channels are defined. Different optode templates for different probe design can be stored in one single .xml file. The physical cap was self-made from a swimming cap. With the help of a dummy head model, correct positions of the optodes were marked and holes were drilled accordingly. The mounts were put on the cap on the holes. In order to ensure the correct channels length to be fixed exactly at 30 mm, plastic holders were also placed on the long channels. As for the short channels, the package comes with mounts for short channels. Thus, no plastic holders were needed in the case. The short channels were 11 mm long. The self-made cap turned out to work out well. The contacts between the scalp and the optodes were good thanks to the elastic characteristic of the material.

## **2.3 Acoustic Stimulation during fNIRS Experiment**

Auditory stimuli were delivered binaurally via an audio metric headphone (Sennheiser HD 650). Stimuli consisted of 20-s chunks of the ICRA noise [Dreschler et al., 2001].

To begin with, ICRA noise was developed to be used as background noise in clinical tests of hearing aids and possibly for measuring characteristics of non-linear instruments. The signals are based on live English speech from the EUROM database [Chan et al., 1995] in which a female speaker is explaining about the system of arithmetical notation. The speech signals were sampled with a sampling rate of 44.1 kHz. By composing the speech signals with well defined spectral and temporal characteristics, the modified signals have long-term spectrums but are completely unintelligible.

We chose to use ICRA noise as stimuli based on several reasons. For one, ICRA noise is broadband amplitude-modulated signal. By selecting a broadband stimulus, broad cortical auditory areas are activated more strongly compared with simple static stimulus. The bandwidth of auditory stimuli is

## *Methods*

positively correlated with the mean percentage signal change and spread of cortical activation [Hall et al., 2001]. Previous fMRI study also manifested that more complex auditory stimuli elicit greater response in most parts of the auditory cortes [Belin et al., 2002]. For the other, ICRA noise is a well-known and accessible stimulus. It is also considered as an international de facto standard for hearing research. In this way, our results can be comparable with other researches.

As for choosing different sound level pressure, we picked 40 dB, 65 dB, 90 dB, and silent stimulus, i.e. 0 dB. Calibrations were performed using an oscilloscope, a G.R.A.S. Power Module Type 12AK, and an artificial ear (G.R.A.S. 43AA). The artificial ear transform the SPLs (sound pressure levels) into electrical signals, i.e. voltages that can be measured by the oscilloscope. According to the instruction manual of the G.R.A.S. artificial ear, the measured level is 11.19 [ $\frac{mV}{Pa}$ ] and we know the SPL in dB is defined as

$$SPL[dB] = 20 \cdot \log \frac{P}{P_0}, \text{ where } P_0 \text{ is } 20\mu\text{Pa}$$

Hence, the relation between SPL and measured voltage should be.

$$V = 20\mu Pa \cdot 10^{\frac{SPL}{20}} \cdot 10^{\frac{Gain}{20}} \cdot 11.19 \frac{mV}{Pa}$$

The headphone with the artificial ear were setup together in the sound booth to ensure minimal environmental noise. The output voltages were measured with the oscilloscope. This way, the corresponding amplitude inputs for later MATLAB scripts for the desire SPLs can be determined.

MATLAB and Oxysoft were used during the measurement. In MATLAB, a chunk in the ICRA audio files was selected. It was multiplied with different amplitude levels for 4 SPLs and ramped by a 10-ms Hanning window. In each epoch, all four stimuli (0dB, 40 dB, 65 dB, and 90 dB) were played randomly once. After each stimulus, there was a 25-sec silence rest to wait for the hemodynamic response. For each participant, 8 epochs were conducted. The stimuli were marked with Labstreaminglayer to note which SPL it was. This Labstreaminglayer also acted as an interface between MATLAB and Oxysoft, so that Oxysoft could mark the time for each stimulus in the measurement data correctly in real time.

## **2.4 fNIRS Setup**

The Brite23 was used in this research. It is light weight, has 10 sources and 8 detectors and can support up to 23 channels. The Brite23 fNIRS

## 2.5 Data preprocesing

device was connected via bluetooth to the PC and the Oxysoft software. For each measurement, the DPF is calculated depends on the age of the participant. The sampling rate was fixed at 50 Hz, for enough resolution but not unnecessary too large in terms of data size.

After the setting in the Oxysoft software was done, the participant would be asked to put on the self-made cap. On each optode position, the hair would be put aside gently with a Q-tip to ensure better contact between the optodes and the scalp. Then, the participants would be asked to put on the headphone and go into the sound booth. The participants were also asked to keep the eyes closed and keep the head still to ensure minimum interference from visual stimulation and motion artifact.

## 2.5 Data preprocesing

Data preprocessing and analysis was executed in MATLAB (Mathworks, USA) and the Homer3 toolbox. The following steps were executed.

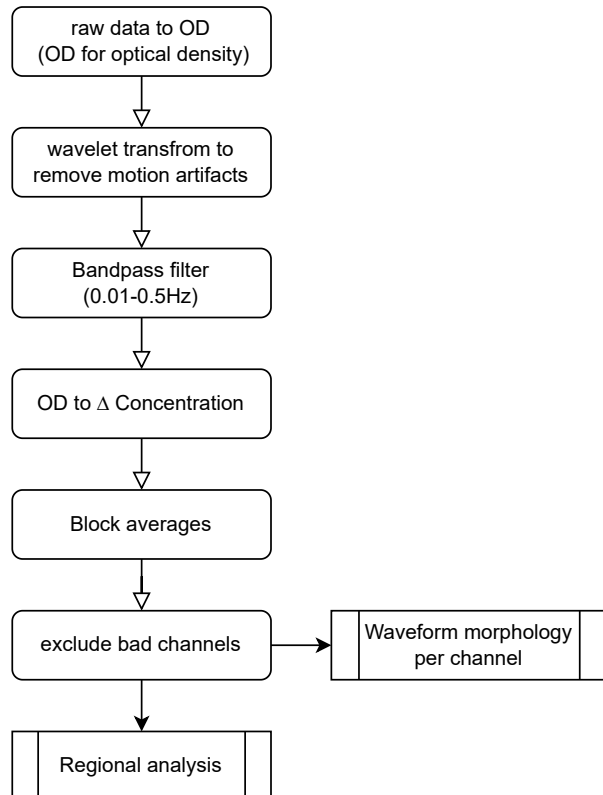


Figure 2.6: Flow Chart of Data Processing

## *Methods*

First, the hemodynamic response was extracted with the Homer3 toolbox. Raw data were converted into optical densities. Motion artifacts were removed by using wavelet transformation of the data. [Molavi and Dumont, 2012]. We also tried to use principle component analysis (PCA) to remove motion artifact, since PCA has the advantage of faster computation. However, it is also known for tending to remove too much of the activation signal in adults. Wavelet transform on the other hand, takes longer to compute, but it is better at maintaining frequency content. And then, the Homer3 toolbox bandpass filter [0.01 - 0.5 Hz] was used to reduced drift, broadband noise, heartbeat, and respiration artifacts. Changes of concentration of oxygenated and deoxygenated hemoglobin were estimated by applying the modified Beer-Lambert Law [Delpy et al., 1988]. In this step, a correction factor, DPF, is used. Although strictly speaking, the DPF should be experimentally obtained with FD-NIRS or TD-NIRS, due to device limitation, it is not possible in this project. Hence, in our research, the DPF was determined by wavelengths of the fNIRS device and age of the participant. [Duncan et al., 1996]. With the given literature, the DPF for two wavelength is calculated with the formulas:

$$DPF_{744} = 5.11 + 0.106 \cdot Age[yr]^{0.723}$$

$$DPF_{852} = 4.67 + 0.062 \cdot Age[yr]^{0.819}$$

Duncan et al. developed a broadband radiofrequency-modulated PRS instrument using four wavelengths(690, 744, 807, and 832 nm) which can measure phase shifts through more than 4 cm of brain tissue in less than 1 s. In the study, the modulation frequency was set at 200 MHz, which has been shown theoretically to be a frequency at which phase shift and true mean optical path length are equal [Arridge et al., 1992]. By dividing the true mean optical path length with source detector separation, the DPF can be obtained.

The authors also provided mathematical models based on the measurements. The estimated DPF is in a sequential order as the used wavelengths. The shorter the wavelength, the larger the mean DPF they measured. Even though only 4 equations were provided with the above-mentioned 4 wavelengths, and our wavelengths are different then that of the authors used, we are convinced that with the above two equations, we may still get fair estimate of the true DPF in our case.

## 2.5 Data preprocesing

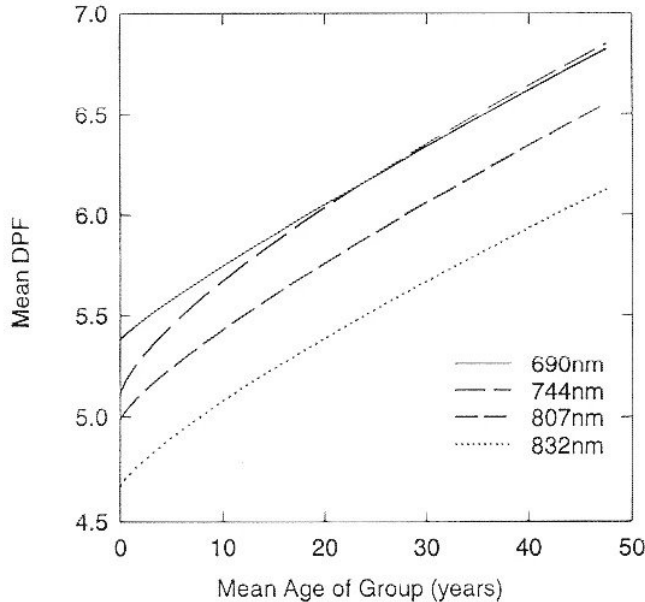


Figure 2.7: Age dependence of DPF. From Duncan et al.

It is important to note that the noise due to motion artifacts, drift, broadband noise, heartbeat, and respiration artifacts need to be processed before the concentration was estimated, according to the previous research [Huppert et al., 2009].

Later on, the extracerebral component in long channels should be reduced by using measurements from the short channels as follows: the first principal components from the two short channels were estimated and then multiplied by its coefficient from the GLM (general linear model). However, this is not done in the scope of this research. The coefficient from the GLM were very small. They were of the magnitudes  $10^{-16}$ , whereas the hemodynamic response in the long channels were of the magnitudes  $10^{-5}$ . Hence, we concluded the extracerebral components in our case can be negligible.

Channels with unusable data were excluded here for further analysis. The scalp coupling index (SCI) is a common measure in this case. It is originally described in [Pollonini et al., 2013]. In short, the SCI estimates the correlation between the two wavelength channels in the cardiac band as the following:

First, the signal is bandpass-filtered to keep only the cardiac band. In our case, a wide band of [0.5 - 2.5] Hz was chosen. Then, amplitude normalization is performed, and the SCI computation is defined as the absolute cross-correlation value at 0-time lag.

## *Methods*

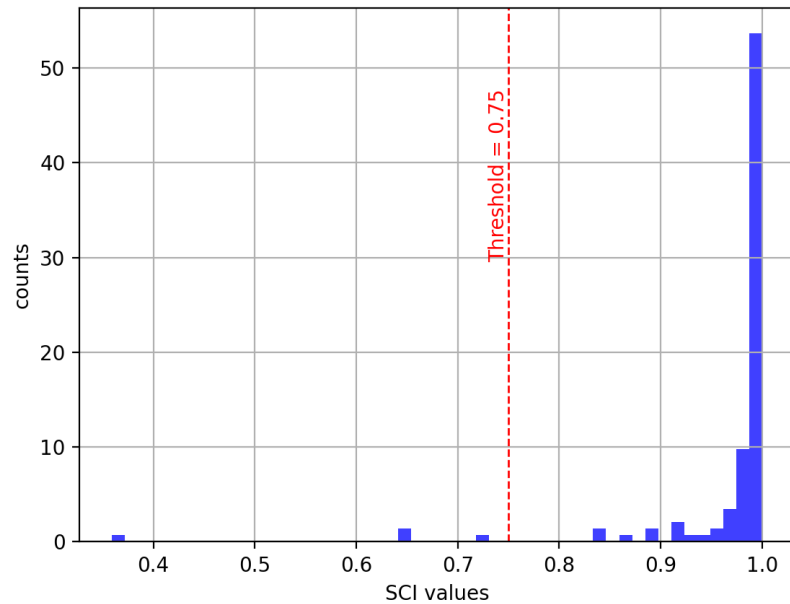


Figure 2.8: Distribution of SCI values.

In this project, only 4 channels failed to reach the threshold = 0.75. In other words, of all the measurements (14 channels per participant, 8 participants in total.) That means over 96% of the measurements passed the SCI threshold.

# Chapter 3

## Results

### 3.1 Waveform Morphology

From our measurements, the results varies a lot individually. Hence, grand average and further statistical analysis won't be well-applicable. In this section, waveform morphology of the 14-channel measurements for some of the participants are shown and described.

First of all, our channels with the optode template are defined as this figure.

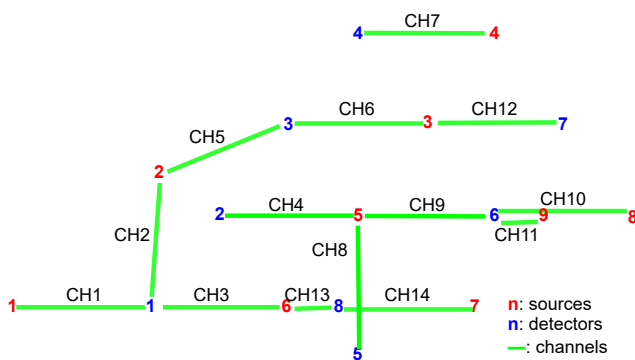


Figure 3.1: channel definition

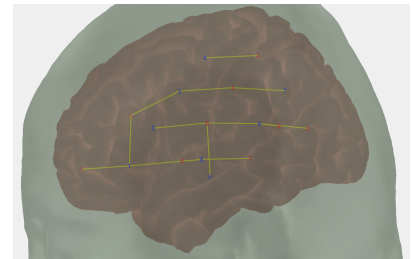


Figure 3.2: on  
AtlasViewer

In the following figures. Channels with invalid SCI won't be taken into consideration, and hence are not shown. Measurements in all channels are plotted in the same scale except for the two short channels marked in thicker outlines. In all our measurements, the changes in the dynamic hemoglobin

## Results

response are significantly less in the short channels by more than a magnitude.

### 3.1.1 Oxygenated Hemoglobin, HbO

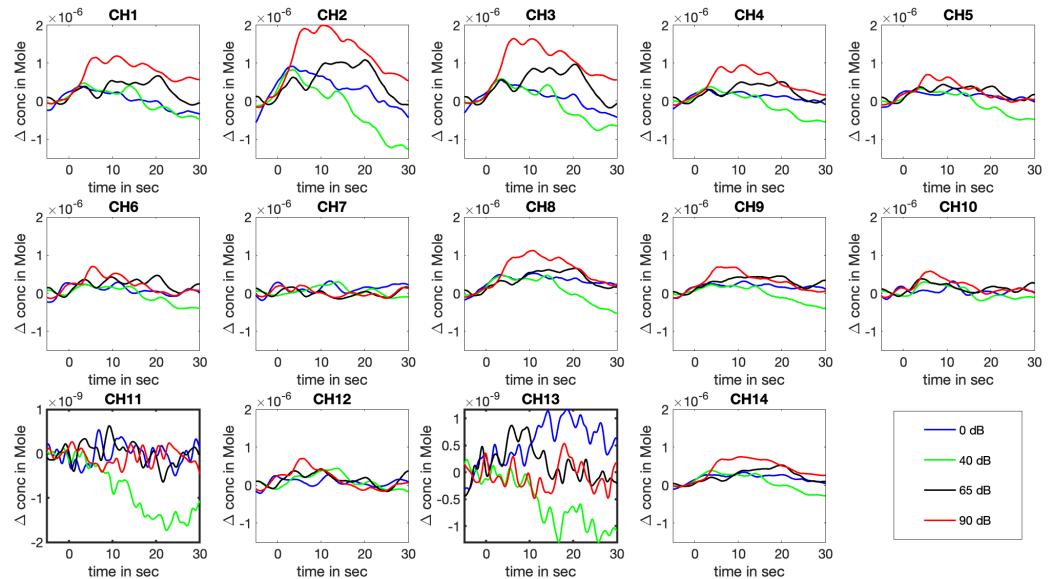


Figure 3.3: Measurement from participant 3.

### 3.1 Waveform Morphology

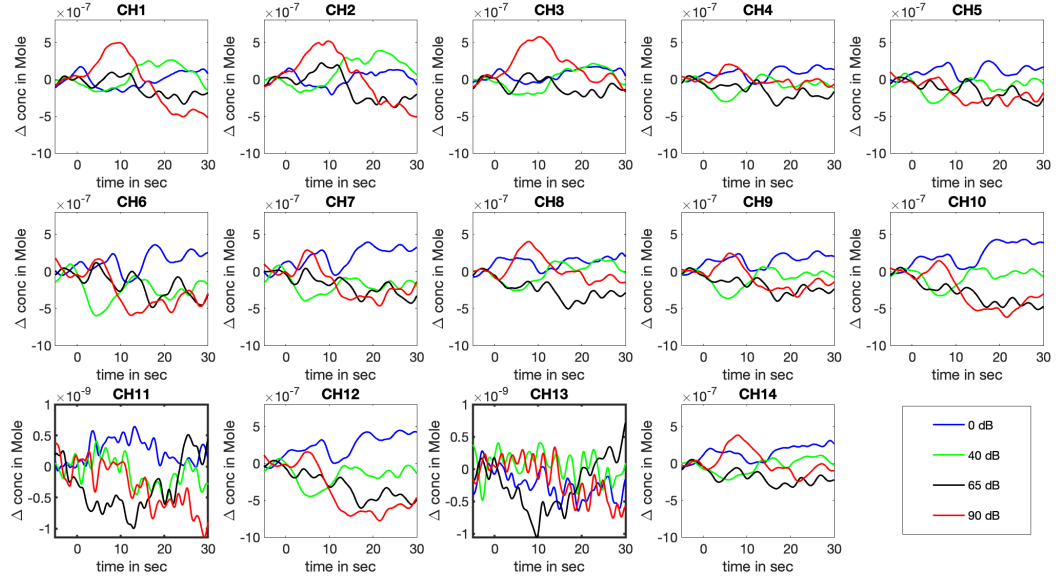


Figure 3.4: Measurement from participant 5.

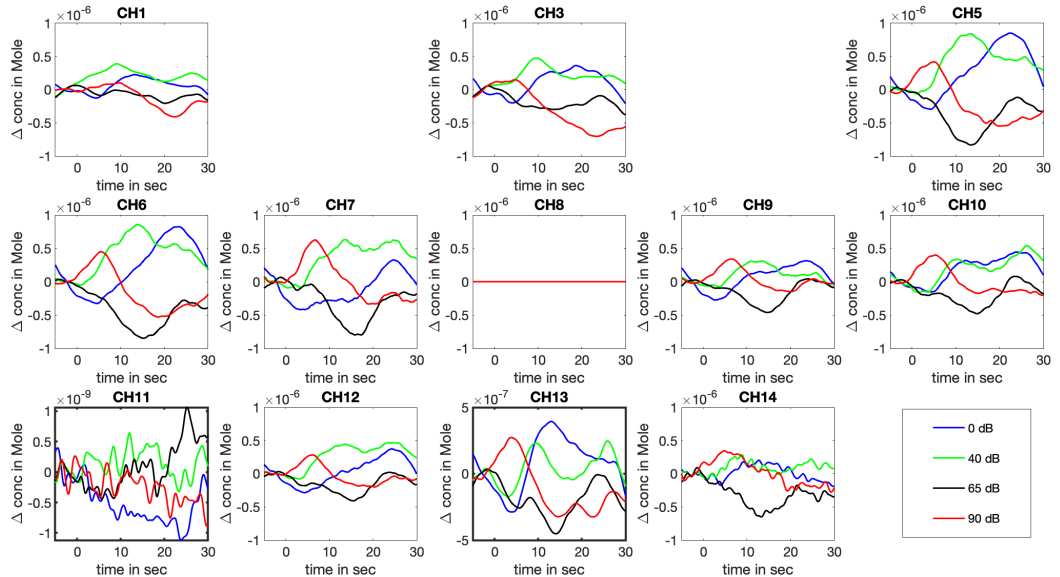


Figure 3.5: Measurement from participant 6.

## Results

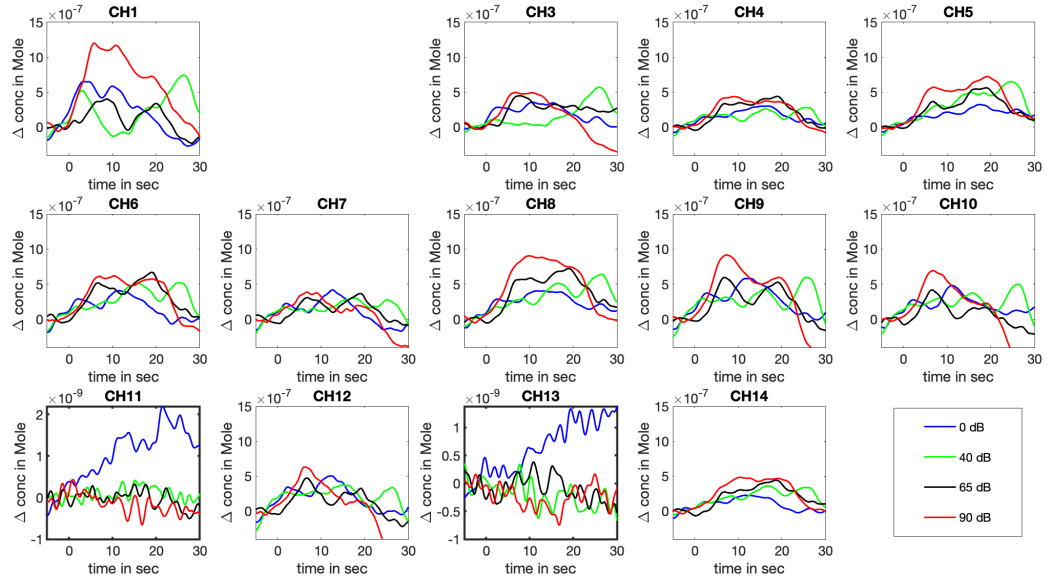


Figure 3.6: Measurement from participant 7.

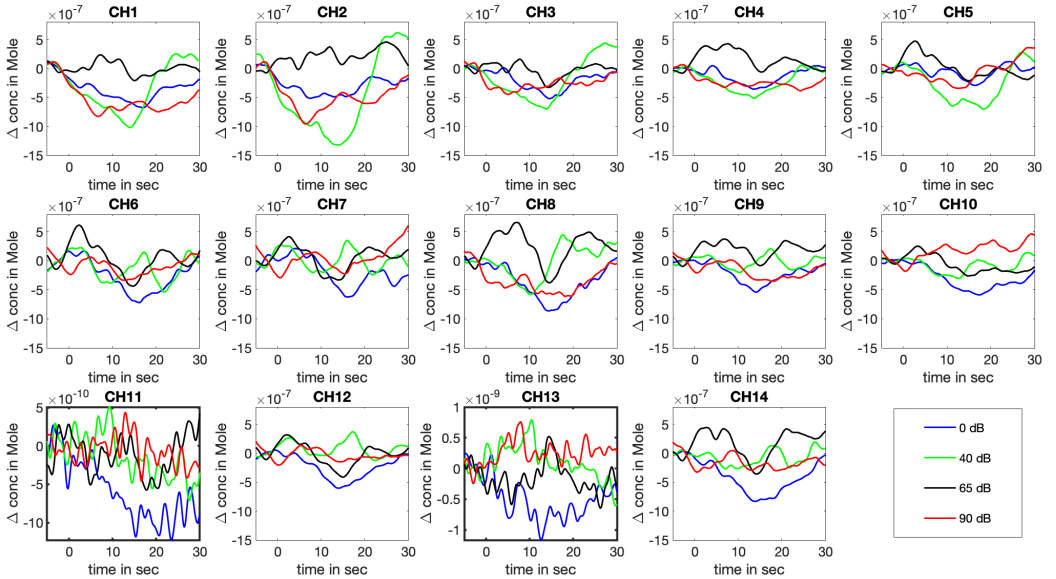


Figure 3.7: Measurement from participant 8. Silent comparison

### 3.1 Waveform Morphology

#### 3.1.2 Deoxygenated Hemoglobin, HbR

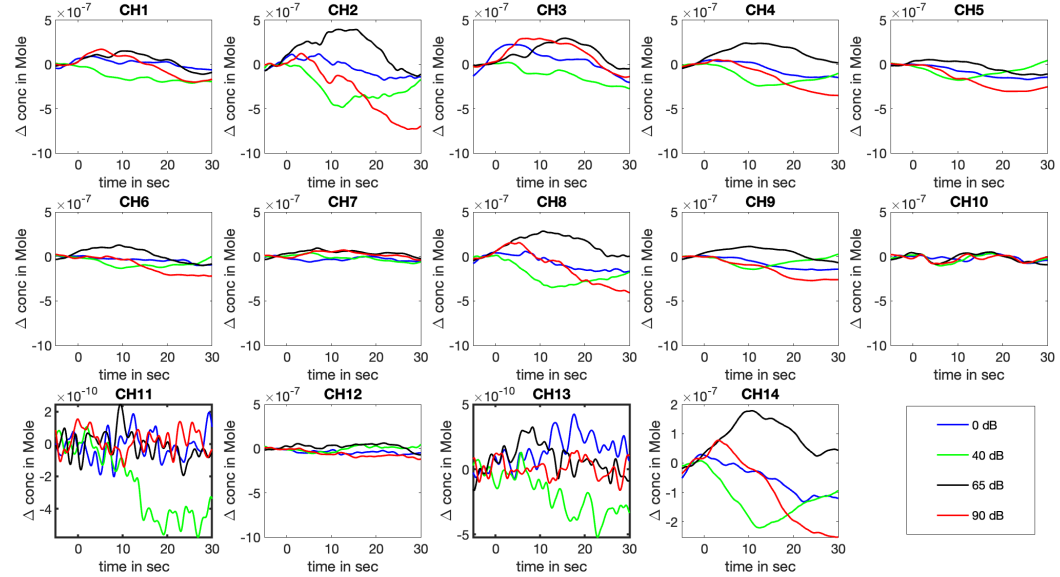


Figure 3.8: Measurement from participant 3.

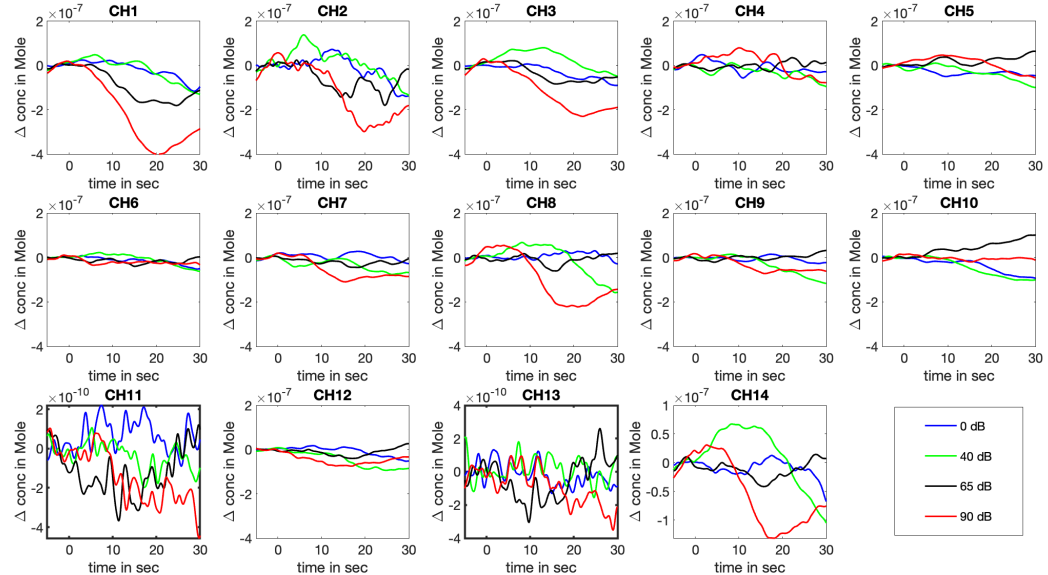


Figure 3.9: Measurement from participant 5.

## Results

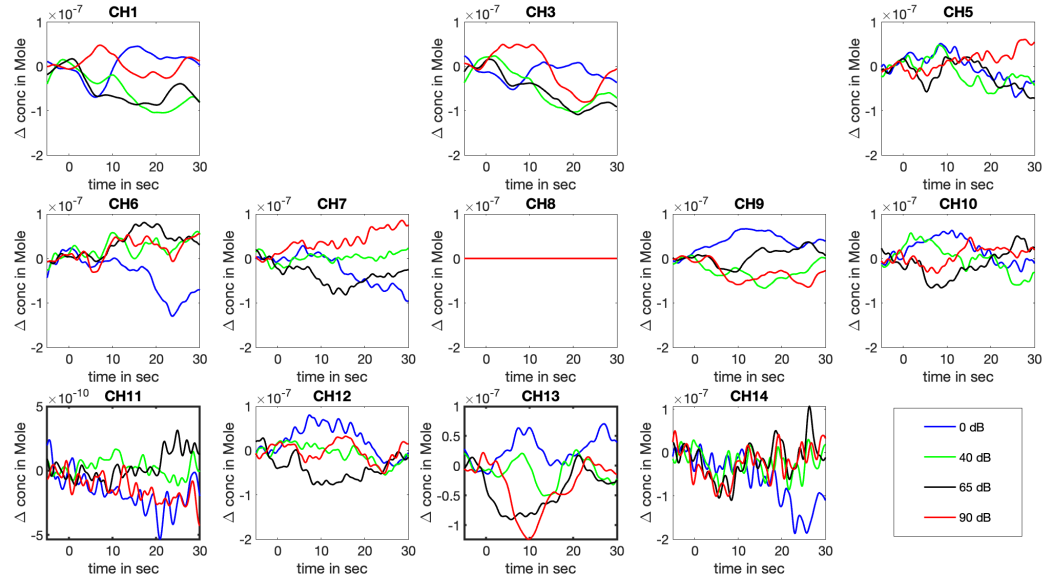


Figure 3.10: Measurement from participant 6.

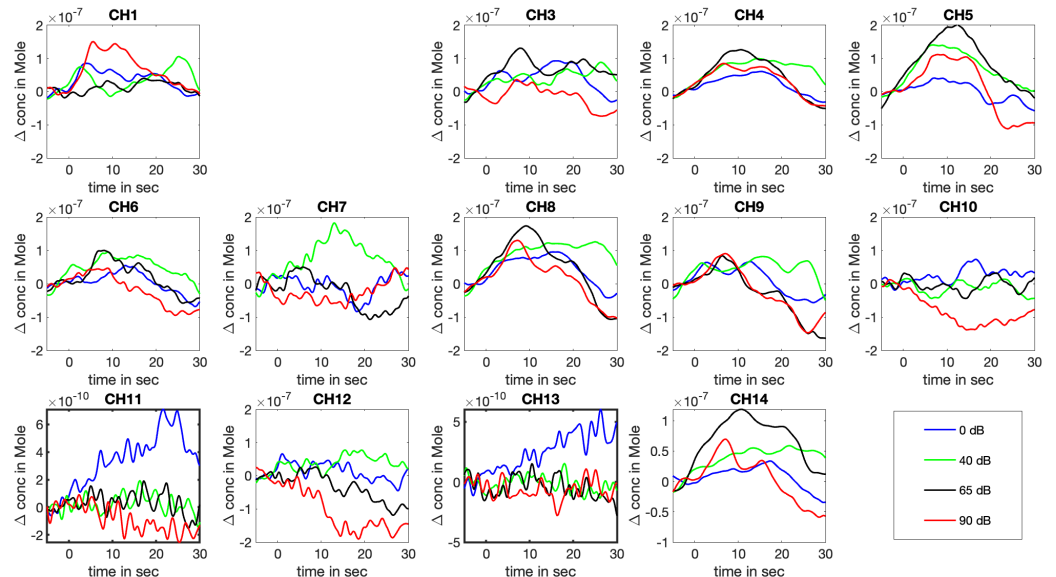


Figure 3.11: Measurement from participant 7.

### 3.2 Region of Interest

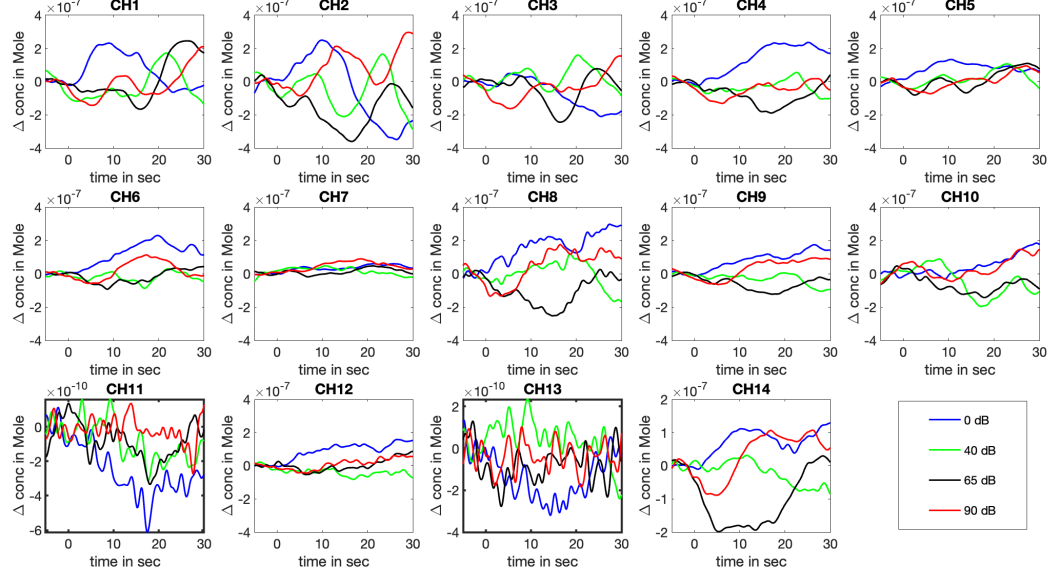


Figure 3.12: Measurement from participant 8. Silent comparison

## 3.2 Region of Interest

In the following, regions of interest (ROI) are defined as the following figures. The auditory cortex is in particular of our interest. Hence, channel 4, channel 8, and channel 9 together formed one region (ROI 2). The rest of the channels formed ROI 1. It is of our interest to compare how the response of the auditory cortex differ from the rest of the left brain hemisphere.

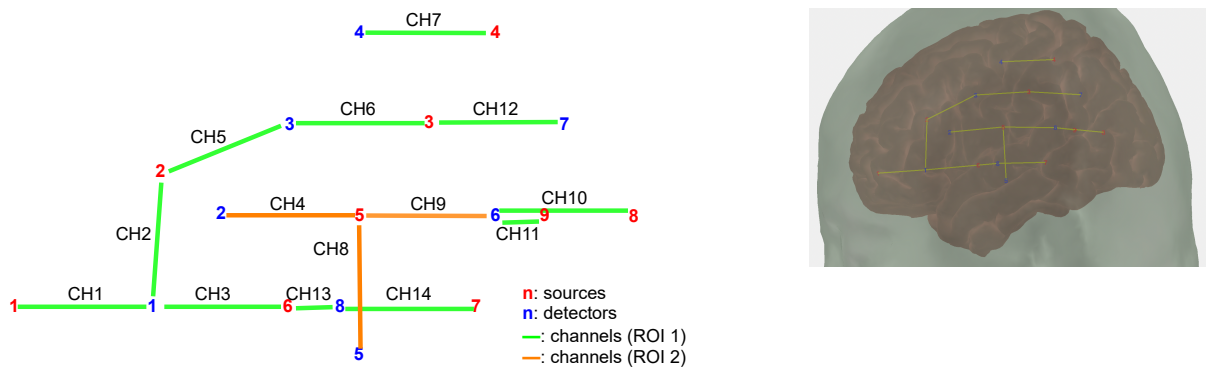


Figure 3.13: channel definition

Figure 3.14: on  
AtlasViewer

## Results

The following plots shows the averaged **HbO** response of all the valid channels in the defined region.

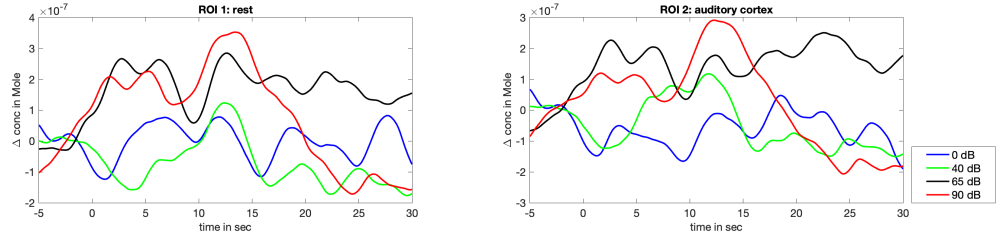


Figure 3.15: Measurement from participant 1.

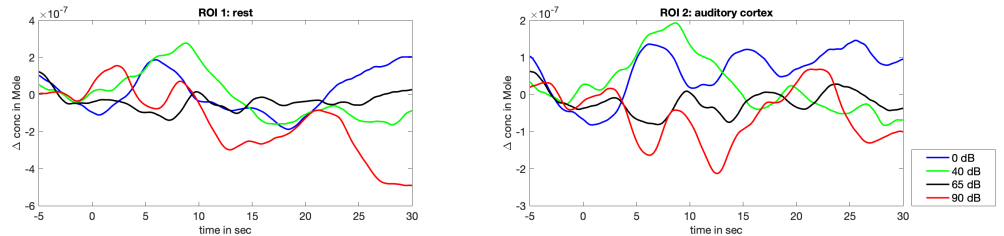


Figure 3.16: Measurement from participant 2.

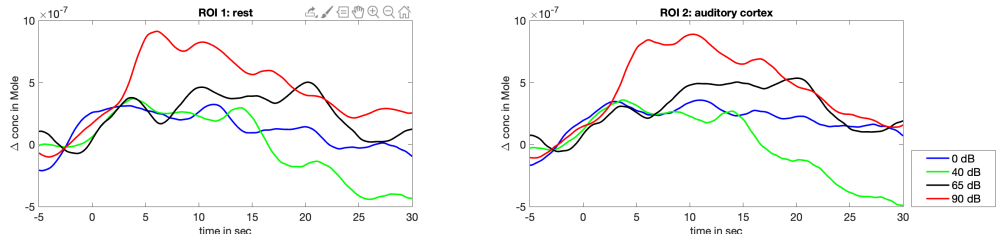


Figure 3.17: Measurement from participant 3.

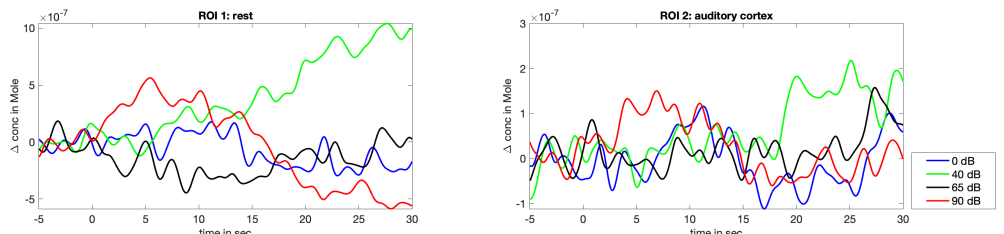


Figure 3.18: Measurement from participant 4.

### 3.2 Region of Interest

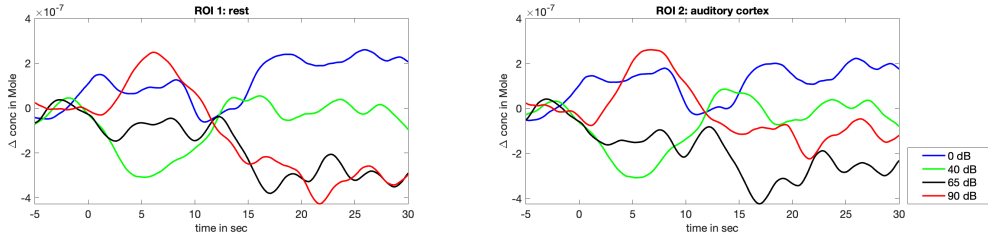


Figure 3.19: Measurement from participant 5.

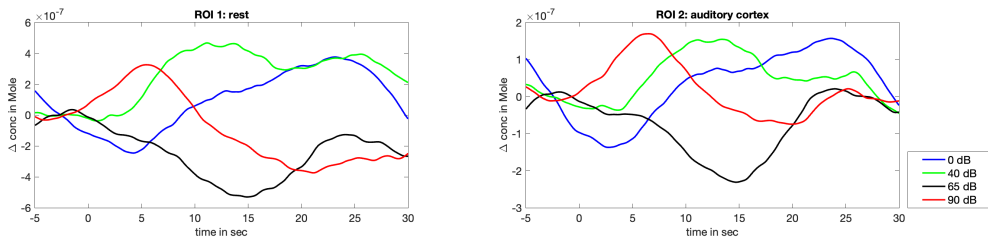


Figure 3.20: Measurement from participant 6.

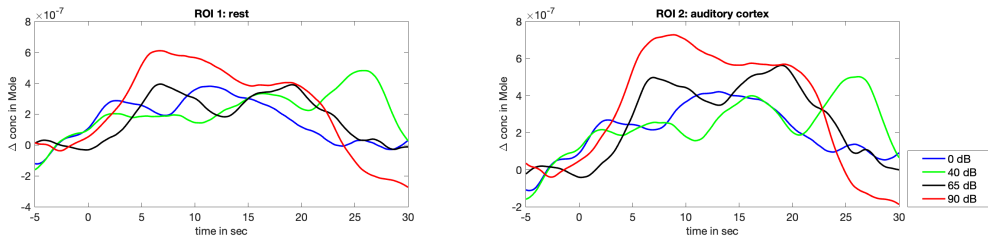


Figure 3.21: Measurement from participant 7.

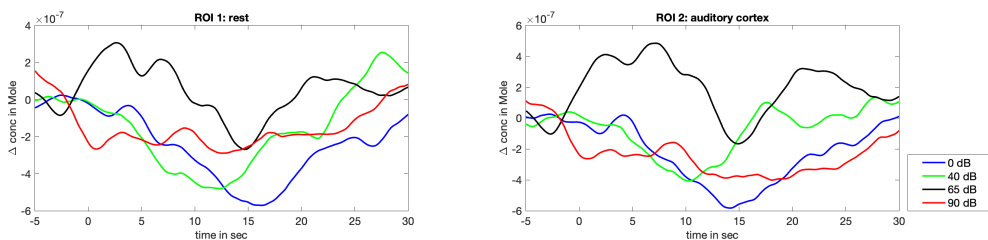


Figure 3.22: Measurement from participant 8. Silent comparision.

## Results

### 3.3 Poor Measurements

There were also some poor measurements even though the SCI is above the threshold 0.75. For example, in our case of participant 4. One possible reason can be due to the thick dark hair of the participant. Light absorption can affect the result greatly.

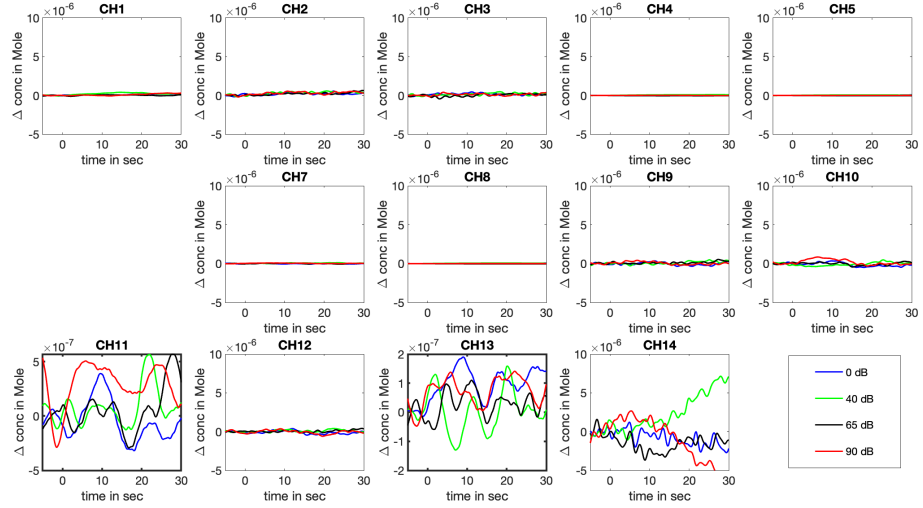


Figure 3.23: HbO Measurement from participant 4.

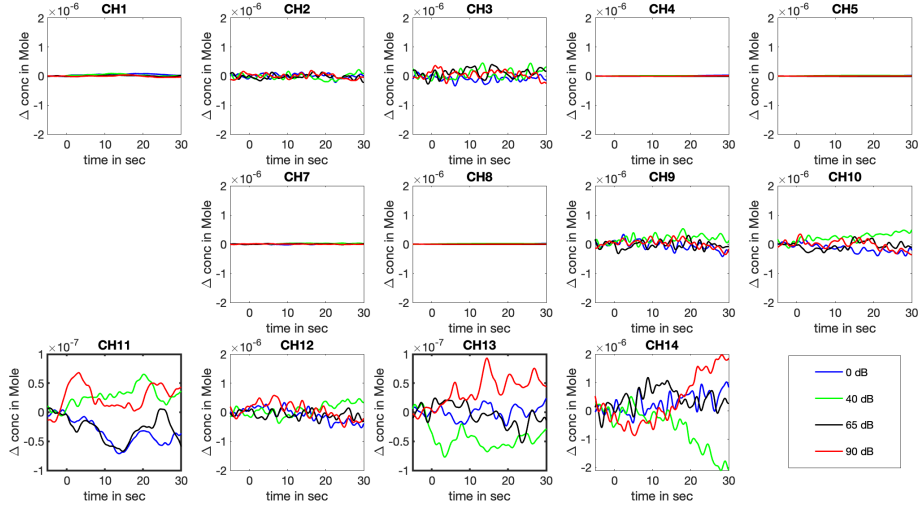


Figure 3.24: HbR Measurement from participant 4.

# **Chapter 4**

## **Discussion**

In this chapter, individual case-by-case study will be discussed in detail. The results from our measurements will also be compared with the counterparts from Weder et al.

### **4.1 Participant 3**

The results from this participant was the closest one to the results reported by Weder et al. For the oxygenated hemoglobin HbO waveform morphology, tonic response could be observed in channel 1, 2, and 3, and phasic response could be observed in channel 10 and 12.

### **4.2 Participant 5**

For the oxygenated hemoglobin HbO waveform, there were significantly larger on-sets for the 90 dB sound stimuli in Channel 1, 2, and 3, i.e. around the Broca's area.

Apart from this, the waveforms for deoxygenated hemoglobin, HbR, were also quite different from the ones Weder et al. reported. For the loudest sound stimuli, channels overlying the caudal superior temporal gyrus and channels over Broca's area showed clear phasic response.

### **4.3 Participant 6**

For the oxygenated hemoglobin, HbO waveform, the loudest sound stimuli resulted in phasic response for almost all the channels. In addition, it also

## *Discussion*

resulted in faster on-set compared with other stimuli of lower sound pressure levels.

On the other hand, as for the deoxygenated hemoglobin, HbR response, results from multiple channels appeared to be noisy even if the SCI values were already above the suggested threshold.

## **4.4 Participant 7**

The results from this participant are rather indeterminant to differentiate between response to different sound pressure levels.

## **4.5 Participant 8**

This participant was given only silence stimuli. No pattern could be concluded for the measured waveform morphology. Nonetheless, it's noteworthy to know that even if there are almost no visual and sound stimuli, dynamic hemoglobin response still exists.

## **4.6 Regional Analysis**

In comparison to the research from Weder et al., we chose a different approach to define our region of interest. Instead of first looking at the results and grouping different regions according to similar waveforms, we were more interested to know how the responses from the auditory cortex would be compared with other regions of the measured left brain hemisphere, so we grouped the three channels over the caudal superior temporal gyrus as one region (ROI 2), and the rest of the channels as another region (ROI 1).

The auditory cortex was our interest of this study. It is around the caudal superior temporal gyrus. We compared the hemoglobin response from the three channels over the auditory cortex with all the other channels lying on the rest of the measured left brain hemisphere. The waveform morphology of the auditory cortex is very similar to the counterparts of the rest of the measured parts. In other words, the dynamic hemoglobin response of the auditory cortex represents that of the entire left brain hemisphere fairly well.

# Chapter 5

## Conclusion and Future Prospectives

In this project, we aimed to confirm and reproduce the results from Weder et al. With the limited devices, we made our measurement conditions, i.e. optode template configuration and audio sound stimuli as similar as those of the previous research from Weder et al. as possible.

The results we got for the waveform morphologies did not speak entirely with the results that Weder et al. reported. In most of the cases, larger sound pressure level did result in greater positive change of oxygenated hemoglobin concentration, or in other words, greater negative change in deoxygenated hemoglobin concentration. However, the results are not consistent between every participants. The separation between different sound pressure levels could not be clearly seen. Apart from the results with the loudest audio stimuli, responses from other quieter audio stimuli were rather indistinguishable. Moreover, regarding the type of responses we measured from different regions of the left brain hemisphere, phasic response could be observed from the channels over the supramarginal superior temporal gyrus from most of the participants. However, only from some of the participants, channels over Broca's area could show a broad tonic pattern as Weder et al. described.

There could be several factors which caused the results from this project to vary from that Weder et al reported. First, we used the device Brite23. It is also a continuous-wave fNIRS device. The sources emitted light of slightly different wavelengths, which are 757 nm and 843 nm, whereas Weder et al. uses the device which sources emitted light of wavelengths 760 nm and 850 nm. Additionally as for the fNIRS testing procedure, we could have also improved on several things. To begin with, a dark sound booth would be more suitable. In our setup, the testing was also performed in a sound booth, but with normal light condition. However, if the lighting was dimmer,

## *Conclusion and Future Prospectives*

there could be less noise in the hemoglobin response from visual stimulation. Additionally, it would make sense to stabilize the participant's neck with a neck cushion. Not only would it be more comfortable for the participants during the measurement. Movement artifacts could also be reduced.

data processing -*j*, almost -*j*, still not yet mentioned the beta and short channel extra cebrelle thingy -*j*dpf

waveform

roi

//future

what could have gone wrong: software different cap position (optode template design and offsets when putting on a cap) mention the broca's area having phasic response (jonas?)

different device, different wavelength

more participants

better understanding of the spatial position with the optode templates (e.g. which channels are over brocas area, which are over supramarginal or caudal superior temporal gyrus, etc.)

# List of Figures

2.1	Probe design from Weder et al. . . . .	5
2.2	Probe design in this research. Shown in AtlasViewer. The red numbers represent the light sources and the blue numbers represent the detector. Channels are shown in yellow lines. . . . .	5
2.4	Manufacturing process of the cap . . . . .	6
2.5	Finished cap on dummy . . . . .	6
2.3	SDgui interface and optode coordinates. . . . .	6
2.6	Flow Chart of Data Processing . . . . .	9
2.7	Age dependence of DPF. From Duncan et al. . . . .	11
2.8	Distribution of SCI values. . . . .	12
3.1	channel definition . . . . .	13
3.2	on AtlasViewer . . . . .	13
3.3	Measurement from participant 3. . . . .	14
3.4	Measurement from participant 5. . . . .	15
3.5	Measurement from participant 6. . . . .	15
3.6	Measurement from participant 7. . . . .	16
3.7	Measurement from participant 8. Silent comparison . . . . .	16
3.8	Measurement from participant 3. . . . .	17
3.9	Measurement from participant 5. . . . .	17
3.10	Measurement from participant 6. . . . .	18
3.11	Measurement from participant 7. . . . .	18
3.12	Measurement from participant 8. Silent comparison . . . . .	19
3.13	channel definition . . . . .	19
3.14	on AtlasViewer . . . . .	19
3.15	Measurement from participant 1. . . . .	20
3.16	Measurement from participant 2. . . . .	20
3.17	Measurement from participant 3. . . . .	20
3.18	Measurement from participant 4. . . . .	20
3.19	Measurement from participant 5. . . . .	21
3.20	Measurement from participant 6. . . . .	21

*List of Figures*

3.21 Measurement from participant 7. . . . .	21
3.22 Measurement from participant 8. Silent comparision. . . . .	21
3.23 HbO Measurement from participant 4. . . . .	22
3.24 HbR Measurement from participant 4. . . . .	22

# List of Tables

2.1 Study Participants. . . . .	4
---------------------------------	---

# Bibliography

- [Aasted et al., 2015] Aasted, C. M., Yücel, M. A., Cooper, R. J., Dubb, J., Tsuzuki, D., Becerra, L., Petkov, M. P., Borsook, D., Dan, I., and Boas, D. A. (2015). Anatomical guidance for functional near-infrared spectroscopy: AtlasViewer tutorial. *Neurophotonics*, 2(2):020801.
- [Arridge et al., 1992] Arridge, S. R., Cope, M., and Delpy, D. T. (1992). The theoretical basis for the determination of optical pathlengths in tissue: temporal and frequency analysis. *Physics in Medicine and Biology*, 37(7):1531–1560.
- [Belin et al., 2002] Belin, P., Zatorre, R., and Ahad, P. (2002). Human temporal-lobe response to vocal sounds. *Brain research. Cognitive brain research*, 13:17–26.
- [Chan et al., 1995] Chan, D., Fourcin, A., Gibbon, D., Granstrom, B., Hucvale, M., George, K., Kvale, K., Lamel, L., Lindberg, B., Moreno, A., Mouropoulos, J., and Senia, F. (1995). Eurom - a spoken language resource for the eu. *Proc. Eurospeech*, 1.
- [Delpy et al., 1988] Delpy, D. T., Cope, M., van der Zee, P., Arridge, S., Wray, S., and Wyatt, J. (1988). Estimation of optical pathlength through tissue from direct time of flight measurement. *Physics in Medicine and Biology*, 33(12):1433–1442.
- [Dreschler et al., 2001] Dreschler, W., Herschuure, H., Ludvigsen, C., and Westermann, S. (2001). Icra noises: Artificial noise signals with speech-like spectral and temporal properties for hearing aid assessment. *Audiology*, 40:148–157.
- [Duncan et al., 1996] Duncan, A., Meek, J., Clemence, M., Elwell, C. E., Fallon, P., Tyszczuk, L., Cope, M., and Delpy, D. T. (1996). Measurement of cranial optical path length as a function of age using phase resolved near infrared spectroscopy. *Pediatric Research*, 39:889–894.

## Bibliography

- [Frost et al., 1999] Frost, J. A., Binder, J. R., Springer, J. A., Hammeke, T. A., Bellgowan, P. S., Rao, S. M., and Cox, R. W. (1999). Language processing is strongly left lateralized in both sexes. evidence from functional MRI. *Brain*, 122 ( Pt 2):199–208.
- [Hall et al., 2001] Hall, D., Haggard, M., Summerfield, A., Akeroyd, M., Palmer, A., and Bowtell, R. (2001). Functional magnetic resonance imaging measurements of sound-level encoding in the absence of background scanner noise. *The Journal of the Acoustical Society of America*, 109:1559–70.
- [Huppert et al., 2009] Huppert, T. J., Diamond, S. G., Franceschini, M. A., and Boas, D. A. (2009). Homer: a review of time-series analysis methods for near-infrared spectroscopy of the brain. *Appl. Opt.*, 48(10):D280–D298.
- [Jöbsis, 1977] Jöbsis, F. F. (1977). Noninvasive, infrared monitoring of cerebral and myocardial oxygen sufficiency and circulatory parameters. *Science*, 198(4323):1264–1267.
- [Molavi and Dumont, 2012] Molavi, B. and Dumont, G. A. (2012). Wavelet-based motion artifact removal for functional near-infrared spectroscopy. *Physiological Measurement*, 33(2):259–270.
- [Pollonini et al., 2013] Pollonini, L., Olds, C., Abaya, H., Bortfeld, H., Beauchamp, M., and Oghalai, J. (2013). Auditory cortex activation to natural speech and simulated cochlear implant speech measured with functional near-infrared spectroscopy. *Hearing research*, 309.
- [Weder et al., 2018] Weder, S., Zhou, X., Shoushtarian, M., Innes-Brown, H., and McKay, C. (2018). Cortical processing related to intensity of a modulated noise stimulus-a functional near-infrared study. *J. Assoc. Res. Otolaryngol.*, 19(3):273–286.

*Bibliography*

# **Erklärung der Selbstständigkeit**

Hiermit versichere ich, die vorliegende Arbeit selbstständig verfasst und keine anderen als die angegebenen Quellen und Hilfsmittel benutzt sowie die Zitate deutlich kenntlich gemacht zu haben.

.....  
Ort, Datum

Pei-Yi Lin